Off-Eutectic Au–Ge Die-Attach — Microstructure, Mechanical Strength, and Electrical Resistivity

Andreas Larsson, Graduate Student Member, *IEEE*, Christian Bjørge Thoresen

***Abstract*—Off-eutectic Au–Ge joints were formed between Si substrates to investigate their high-temperature compatibility. High-quality joints made with small bond pressure, 53 kPa, were fabricated. The joints comprised three different types of morphologies; (1) a layered structure of Au / Au–Ge / Au, (2), a layered structure of Au / Au–Ge / Au where some sections of the central Au–Ge band has been replaced by a Au section that extended across the entire section, and (3) a roughly homogenous Au layer comprising the primary α phase. The average Ge concentration was 10 ± 2 at.%. Joints formed with a higher bond line pressure, 7.6 MPa, were of a reduced quality with voids and cracks at the original bond line. Annealing at 400 °C for 1000 hours transformed the microstructure into a Au–Ge–Si compound with Au precipitates. The shear strength of the fabricated joints was found to be at least 50 MPa, and the fracture mode was an adhesive fracture between the adhesion layer and the die or substrate. Heated dies detached from the substrates at 460 °C, i.e., more than 100 °C above the eutectic melting point of the binary Au–Ge system. Electrical resistivity measurements confirmed a melting process at the eutectic melting point by an abrupt increase in resistivity.**

***Index Terms*—Off-eutectic bonding, Au–Ge die-attach, High temperature**

I. Introduction

MANY industries and applications call for electronics that can operate reliably in high-temperature environments. Such applications include; downhole instrumentation systems in oil and gas recovery, power electronics and control systems for electrification of vehicles and aircraft, and sensors systems for space explorations. The maximum requested operation temperature may go from around 200 °C up to several hundreds of degrees. In recent years, high-temperature compatible components have been developed and demonstrated to operate at high temperatures, 250 °C or more, such as silicon on insulator (SOI), gallium arsenide (GaAs), gallium nitride (GaNi), and silicon carbide (SiC) semiconductive devices. Together with ceramic substrates, such as; alumina (Al2O3), aluminum nitride (AlN) and silicon nitride (Si3N4), and a suitable die attach they form a basis for high-temperature compatible electronics.

Regular lead-tin (Pb–Sn) and more modern lead-free tin-silver-copper (SAC) based solders are not suitable for high-temperature applications, despite recent efforts to extend their maximum operation temperature [1], [2]. Extensive research on high temperature joining technologies for electronics has been undertaken in recent times [3]–[13]. Traditionally, hard solders, or brazes, have been used in high-temperature applications. Their use has typically been limited by their relatively high process temperature when applied to regular Si-based devices, due to their high melting point. To avoid high process temperatures, two diffusion type joining technologies have been adapted for electronic applications; transient liquid phase (TLP) [14]–[18] also often referred to as solid-liquid interdiffusion (SLID) [19]–[21] bonding, and sintering [22]–[24]. These technologies have in common that they can create joints that may withstand higher temperatures than the process temperature that was required to form them. TLP type joints are formed by a solid and liquid interdiffusion process of two (or more) dissimilar adjoined metals. By isothermal solidification of a liquified phase, a homogenous solid-solution (TLP) or an intermetallic compound (SLID) is formed. This new material compound can have significantly different properties than the materials that were used to from it, e.g., an increased melting point. Perhaps the most prominent downside to TLP-type joints is an extended homogenization process step, often requiring hours or days of heat treatment before completion [18]. Such long annealing process steps may be costly. The time to complete homogenization of the joints is linked to the diffusion length. Thus, layered micro-sized joints can reduce this time significantly. Another approach to reducing the processing time even further is to from joints from pastes with dissimilar particles that react with each other forming new phases. Although joints made from pastes often struggle with significant voiding. Sintering, on the other hand, utilize micro- or nano-sized particles that reduce the necessary process temperature required to initiate and sustain sintering between

Submitted 31 January 2019. This work was supported by TECHNI AS, TEGma AS and the Research Council of Norway. Project No.: 244915.

A. Larsson is with TECHNI AS, Dept. of Applied Physics, Borre, NO-3184, NORWAY, and the University of South-Eastern Norway, Dept. of Microsystems, Borre, NO-3184, NORWAY (e-mail: andreas.larsson@techni.no and andreas.larsson@usn.no).

C. B. Thoresen is with the University of South-Eastern Norway, Dept. of Maritime Operations, Borre, NO-3184, NORWAY (e-mail: christian.thoresen@usn.no)

adjoining particles. Usually, high pressures, several to tens of MPa, is required to form strong joints and to reduce the final void fraction in the joints [24]. Thus, fragile components, such as microelectromechanical systems, or MEMS devices, may struggle to cope with the applied mechanical load during bonding. Moreover, the requirement for complex equipment that can apply such loads may be undesirable.

Now that new high-temperature compatible semiconductive devices and ceramic circuit boards exist, e.g. direct bonded copper (DBC) and active metal braze (AMB), hard solders appear to have regained interest for use in high temperature applications due to their relatively simple bonding process with short process times and no requirement for high-pressure equipment [25]. In particular, eutectic gold based joints made with gold–germanium (Au–Ge), gold–silicon (Au–Si) and gold–indium (Au–In) have demonstrated significant strength capacity at very high homologous temperatures ranging between 40–160 MPa at a homologous temperature between 0.8 to 0.9 for eutectic Au–Ge joints [6], [26], [27]. It has also been demonstrated that that off-eutectic Au–Ge joints with 8 at.% Ge have some structural strength at temperatures well above the eutectic melting point [28]. Eutectic Au–Ge joints have also shown great thermal cycling capacity between temperature extremes [29]–[31] as well as microstructural stability when exposed to high temperatures [26]. Thus, joints created from off-eutectic Au–Ge compounds holds potential for forming high-temperature compatible joints that might be used at temperatures exceeding the eutectic melting point, i.e., in a partially liquid state. The term off-eutectic used here is not to be confused with "off-eutectic" bonding sometimes improperly referred to in the pertinent literature regarding TLP and SLID bonding.

This article investigates how two different applied bond line pressures and how annealing at very high temperature affects the joint composition and microstructure. Shear testing at room temperature was used to quantify the strength of the fabricated joints. Fracture analysis was performed on the sheared samples. The effective melting point was evaluated. The work presented in this article builds on the work previously published in [25]. It presents a characterization of the electrical resistivity from room temperature to slightly above the eutectic melting point to investigate how partial melting affects the electrical resistivity.

II. Methods and Materials

A. Materials and fabrication

Samples for process evaluation, shear testing, and cross sections were fabricated by sandwiching a eutectic Au–Ge preform between a die and substrate, both of Au metalized silicon (Si). Heat and pressure were then applied to melt the preform to form a joint. The process from Si wafer to a bonded sample was as follows. A 525 ± 25 µm thick Si wafer (Si-Mat) was oxidized (Harmbridge HiTech, dry, 1100 °C) with a 305 ± 5 nm thick silicon dioxide (SiO_2) layer. A 25 ± 5 nm thick titanium (Ti) (Kurt J. Lesker Company, 99.995 %) adhesion/diffusion barrier layer was deposited onto the SiO_2 surface by electron-beam physical vapor deposition (e-beam)

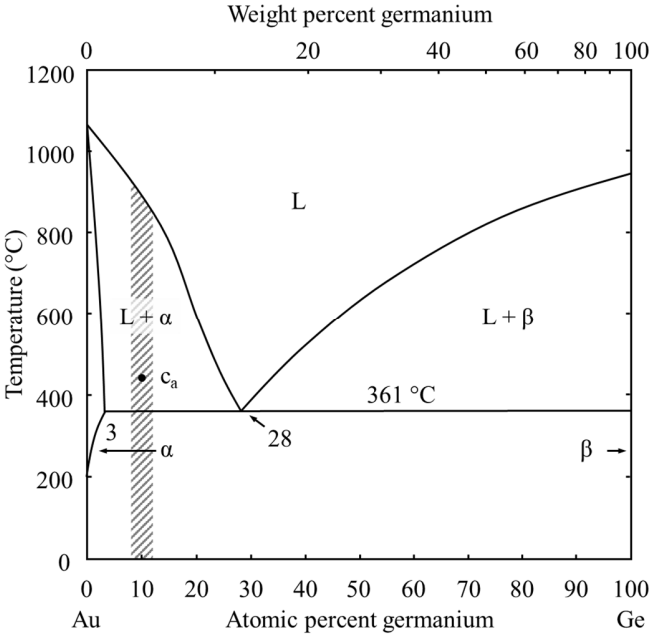

Fig. 1 The binary phase diagram of the Au–Ge system. The target off-eutectic composition of the fabricated joints is marked with a dashed region. The phase diagram was adapted from Okamoto and Massalski [40]. Note that the eutectic isotherm varies slightly in the pertinent literature; 356–361 °C [41], [42].

(A300 A3CV&CTM, 7000 V, 25-40 mA, 5-8·10^{-3} mTorr, 0.3-0.6 A/s) followed by a 160 ± 10 nm thick Au (KA Rasmussen, 99,99 %) layer that was magnetron sputtered (Telemark 294, 35-50 W, argon (Ar) 10 cm^3/min, 3.5–6.5 mTorr, ~23 °C) onto the Ti surface without breaking the vacuum in the sputtering equipment (AJA Int. Phase II J.). The final Au layer thickness was built up by electroplating, using a gold cyanide solution (60 °C to 65 °C, 2.7 mA/cm^2). The final thickness of the Au layer was 22 ± 2 µm. Square dies and substrates, 3.6 mm^2 and 15.2 mm^2, were then laser cut (Roffin PL E 25 SHG CL Flex) from the metalized wafer. A 35 ± 2 µm thick eutectic Au–Ge preform (Goodfellow), 28 at.% Ge, was then sandwiched between dies and substrates. The preform was cut into pieces with the same dimensions as the footprint of the dies. The final Au / Au–Ge preform / Au system equates to an overall atomic Au:Ge ratio in the system of approximately 7.6 ± 0.8 at.% Ge. The local concentration of Ge inside the fabricated joints was expected to be slightly higher than this, based on observations during early process development. The expected off-eutectic composition is marked with a dashed region in the binary Au–Ge phase diagram depicted in Fig. 1.

Dies and preforms were manually placed and aligned on top of substrates forming a symmetrical Si / Au / Au–Ge / Au / Si configuration. The stack was clamped together with a spring-loaded ball plunger in a custom-made fixture and placed into a vacuum bonder (Budatec VS160UG). The bond process was carried out in a dry nitrogen atmosphere at ~1 atm. The temperature was raised above the eutectic melting point (356–361 °C) to a local bond line temperature of 370-380 °C to melt the preform. The sample was then cooled to room temperature. The characteristic process parameters used are presented in Table I. Two different fabrication processes with

TABLE I
CHARACTERISTIC PROCESS PARAMETERS USED FOR THE DIFFERENT SAMPLE GROUPS STUDIED IN THIS WORK.

Group	Number of samples	Bond line pressure kPa	Peak temperature °C	Heating rate °C/min	Cooling rate °C/min	Anneal temperature °C	Anneal duration hr
(a)	18	53 ± 13	370 ± 5	25–30	100–110	-	-
(b)	6	7600 ± 550	370 ± 5	25–30	100–110	-	-
(c)	6	53 ± 13	370 ± 5	25–30	100–110	400	1000
(d)	6	0†	400	120	140	-	-
(e)	1	0†	400	120	140	300	144

† Spacers were used

different bond pressures were used. A first group was fabricated with a spring force of 0.2 N and a second group with a force of 29 N. The applied force created an average local bond line pressure of 53 kPa and 7.6 MPa for the two groups respectively. The applied pressure secured a thermomechanical contact between the adjoining components; die, preform, and substrate. In total, 24 samples from the low-pressure group were prepared. Six out of these samples were placed into an oven at 400 °C flushed with dry N_2 and kept there for 1000 hours. Six samples were prepared with the high-pressure process. The group definitions, with characteristic process parameters used for each group, are summarized in Table I.

Samples for the electrical resistivity tests were fabricated from 22 ± 2 µm thick Au foil that was cut into 2-6 mm wide and 6-10 mm long pieces. An equivalently sized, and 35 ± 2 µm thick eutectic Au–Ge preform was then sandwiched between two foils. This equates to an overall atomic Au:Ge ratio in the joint of approximately 5.9 ± 1.4 at.% Ge. The stack was placed onto a hot plate and positioned between two 60 ± 1 µm thick spacers. A piece of 525 µm thick Si wafer was used as a bridge and was placed on top of the stack and spacers. A clamp was then used to compress the entire stack to secure a good thermomechanical contact between the adjoining components during heating. The spacers secured a nearly pressure-less environment, after melting of the preform, as the compound solidified during the cool down sequence. The process was carried out in vacuum; 3-10 mTorr. The fabricated foil was then cut by hand into smaller 400 ± 50 µm wide and approximately 4 mm long pieces for electrical characterization.

B. *Microstructure characterization*

Samples were cross-sectioned, and the microstructure was analyzed by use of optical microscopy (Carl Zeiss Jena Neophot 32, NA 0.9, up to 1000x magnification), and scanning electron microscopy (SEM) (Hitachi SU8230). The samples were prepared for cross-section analysis by two methods. Most samples were molded into epoxy (Struers EpoFix resin and hardener) followed by wet grinding and polishing, and ion milling. The grinding process stopped at 4000 grit grade paper before preparation was continued with wet polishing using a cloth and a 1 µm diamond paste for the last step. The final surface was prepared with flat ion milling (Hitachi IM4000, Ar) to reveal potential voids or other defects possibly concealed by smearing. A few samples were prepared by directly cutting the sample into two halves with a dicing machine (Disco DAD 3220), followed by a finishing cross section step by ion milling (Hitachi IM4000, Ar). The joint composition was evaluated by energy-dispersive X-ray spectroscopy (EDX) (Oxford X-MAX 150).

C. *Effective melting point*

A detachment experiment was devised to investigate the effective melting point. The effective melting point is defined here as the temperature where the joint is unable to carry a small applied shear load. Samples were placed vertically on a hot plate (Watlow, Ultramic 600). A clamp was used to secure a good thermal contact with the hot plate. A 10-gram weight was hung around the die, creating a shear load of 27 ± 1 kPa on the joint. The temperature was then raised above the eutectic melting point. Two different heating regimes were used: (R_1) A ramp-up at 60 °C/min until the samples sheared off, and (R_2) a slower ramp-up at 10 °C/min up to 380 °C and then kept between 370–380 °C until the samples sheared off. The procedure was carried out in air. Since the experiment was carried out in regular clean room conditions, the attached thermocouple had an offset from the actual joint temperature. The joint temperature was calibrated using materials with known compositions and well-defined melting points (such as In, Sn, eutectic Au–Sn and eutectic Au–Ge) and correlating their melting points with the readings on the thermometer. In addition, a piece of the same eutectic Au–Ge preform that was used to fabricate the samples was pressed onto the top surface of the die, verifying that the local temperature inside the joint was above the melting point of the preform used.

D. *Electrical resistivity*

Resistivity measurements were performed on six virgin samples and on one strip each of the gold film and of the preform used to produce the samples. This was done by measuring the geometry of each sample and the resistance through them. The size of each sample was measured by an optical microscope. A lab thickness measurement setup, consisting of a length gauge (Heidenhain MT 60M) mounted to press against a flat rock surface (Microbas), was used to measure the thickness of each sample.

The resistance through a section of each sample was measured during a thermal cycling process that extended past the eutectic melting point, using a 4-point measurement setup. For this measurement, the sample was placed on a piece of aluminum nitride substrate (0.51 mm thick) on a hot plate (thermal chuck) in a probe station (The Micromanipulator Company). Four probes were placed in two pairs, one near each end of the sample. A small sheet of sample glass (0.88 mm thick) was put on top of the sample in the middle section between the probes and forced down with a micromanipulator probe. This was done to maintain good thermal contact between the sample and the substrate and to prevent the sample from buckling when heated.

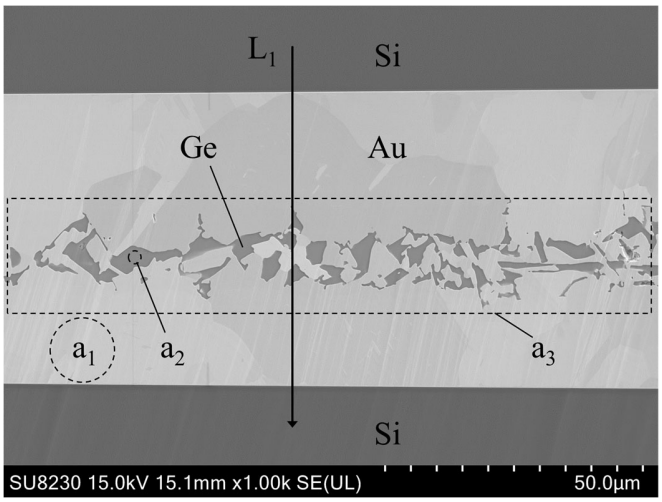

Fig. 2 SEM image of a cross section of a virgin sample from the low-pressure group (a) after joining. A band of explicit Ge domains is in the middle of the joint creating a eutectic band at the original bond line. The composition in regions a_1 to a_3 are given in Table II.

TABLE II
COMPOSITION OF DOMAINS MARKED IN Fig. 2, Fig. 9, AND Fig. 11.

Domain	Composition		
	Au (at.%)	Ge (at.%)	Si (at.%)
a_1	100.0	0.0	0.0
a_2	0.0	100.0	0.0
a_3	64.0	36.0	0.0
A_1	65.1	11.1	23.8
A_2	100.0	0.0	0.0
A_3	100.0	0.0	0.0
A_4	0.0	40.1	59.9

4-point DC resistance measurements using a source meter (Keysight 34972A, 34901A) was used for the two first samples. This setup suffered from high noise at higher temperatures, likely due to variations in the thermoelectric electromotive force at the contacts between the voltage probes and the sample. Therefore, the setup was changed to a lock-in amplifier setup, based on a digital storage oscilloscope (TiePie HS4), with an instrumentation amplifier (AD623) as a differential pre-amplifier. With this setup, the resistance was measured at a frequency of 1.375 kHz and a test current of 2.7 mA.

A thermocouple connected to a data acquisition unit (Keysight 34972A, 34901A) was used for logging the temperature of the hot plate. Due to the thermal resistance between the hot plate and the sample, the temperature measured by this thermocouple was higher than the actual temperature of the sample. An experiment replacing the sample in the setup with a second thermocouple showed a linear relationship between the two measured temperatures, with only a scale factor when measured in °C. However, the thermocouple in this test case does not have the same thermal contact with the glass and substrate as the sample in the resistivity measurements, resulting in a different scale factor for the relationship between the hot plate thermocouple and the sample. Therefore, a scale factor based on the visual observation of the melting of the eutectic Au–Ge in the sample was used to get a more accurate estimate of the actual sample temperature. Data points for resistance and temperature were logged at a rate of 1 Hz.

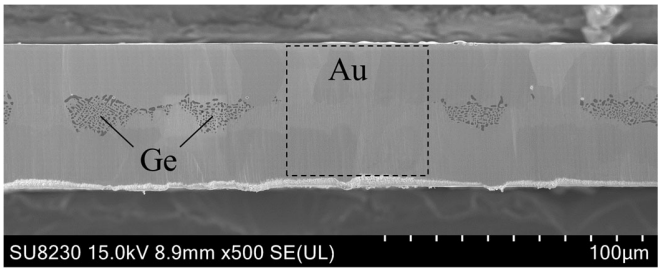

Fig. 3 SEM image of a cross section of a sample for electrical characterization after one hour at 300 °C. A section of primary Au extends through the Ge band in the middle of the image.

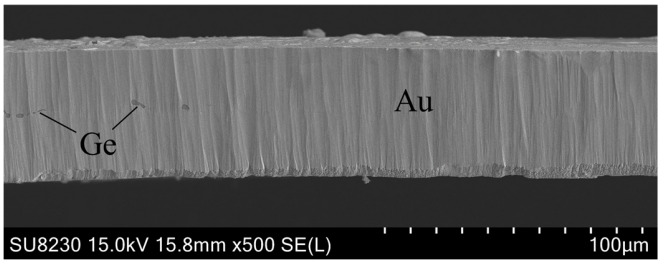

Fig. 4 SEM image of a cross section of a sample for electrical characterization after 16 hours at 300 °C. A section of primary Au phase extends the entire section.

The temperature profile for the resistance measurements consisted of active heating with a hot plate set point of 400 °C for about 30 min, which gave a stable temperature for the last 5 min. Then passive cooling for around 10 min, to reach a temperature of about 270 °C, and finally active cooling down to room temperature. The total cycle time was around 50 min. The probes occasionally suffered a loss of contact, likely due to thermal expansion of the probes and the sample. When this occurred, the ramp up or down was halted until the electrical contact had been reestablished by repositioning the probes on the sample. In order to compensate for the resulting variation in the probe positions, the resistivity calculations were based on measurements of the actual distance between the voltage probes throughout the thermal cycling.

III. RESULTS AND DISCUSSION

A. Microstructure

The fabricated joints from the low pressure, 53 kPa, groups (a) and (d) comprised three characteristic morphologies; (1) a layered structure of Au / Au–Ge / Au as can be seen in Fig. 2, (2), a layered structure of Au / Au–Ge / Au where some sections of the central Au–Ge band has been replaced by a Au section that extended across the entire section as can be seen in Fig. 3, and (3) a roughly homogenous Au layer comprising the primary α phase, shown in Fig. 4. Elemental analysis results of the regions a_1-a_3 marked in Fig. 2 are presented in Table II. EDX maps of the section shown in Fig. 2 are presented in Fig. 5. It is seen that pure Ge domains have segregated into explicit domains in the center of the joint, i.e., at the original bond line, forming a eutectic type band with Au layers on both sides. The overall composition of the virgin joints from group (a) and (d) was found to comprise an off-eutectic Au–Ge compound with 10 ± 2 at.% Ge. The local Ge concentration in sections evaluated typically varied from 1–4 at.% Ge in sections

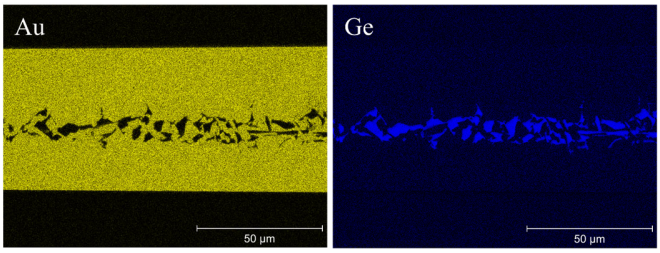

Fig. 5 EDX maps of Au and Ge of the same section as shown in Fig. 2.

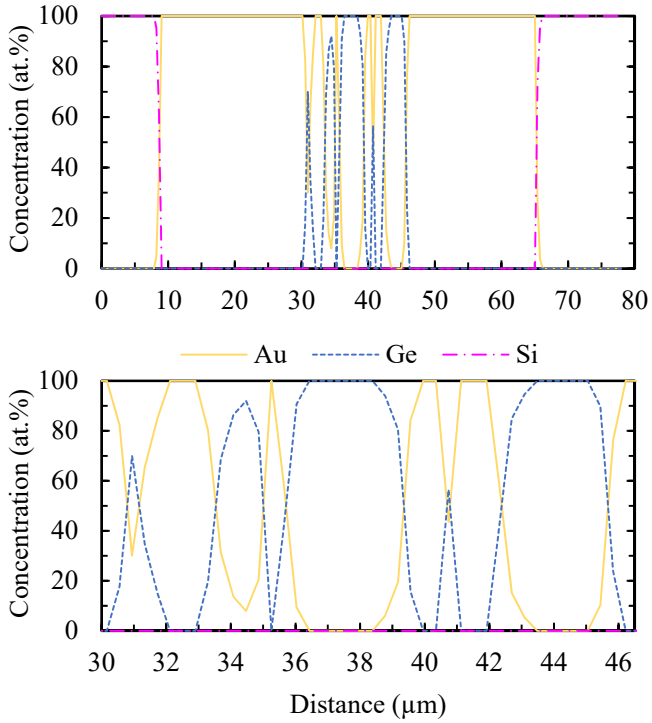

Fig. 6 The top graph shows the component concentration across a virgin joint from the low-pressure group (a). The position of the line scan is indicated by L_1 in Fig. 2. The lower graph shows a magnified section of the concentration change across the Ge band in the middle of the joint.

apparently with only Au, morphology (2), to 10–20 at.% Ge in sections with a central Ge band, morphology (1). Cross sections taken at different locations in the same sample showed different morphologies (1)–(3). This indicates that the morphology was inhomogeneous throughout the entire joint. It is advised to investigate this characteristic in a more detailed study before making conclusions. No Si was found in the joint of the virgin samples from group (a), see Fig. 6. In general, these joints were of high-quality with very few defects. Only a few voids were found. They were likely formed from enclosed gas upon solidification. These voids were ellipsoidal with a smooth and rounded perimeter. They were located at the joints' original bond line and with a characteristic size of a few µm. No cracks or similar features were discovered.

When the bond line pressure was increased to 7.6 MPa, group (b), a significant amount of the eutectic preform was rapidly squeezed out from the bond line upon liquification of the preform. Thus, the joints reminded more of thermo-compression type bonds. At the bond line, Au bridges extend across a visible bond line interface in the middle of the joint, not dissimilar from thermocompression type joints [26]. A band

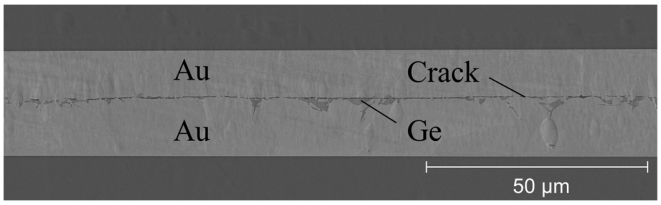

Fig. 7 SEM image of a cross section of a virgin sample from the high pressure, 7.6 MPa, group (b) after joining. An extensive through crack in the center bond line is clearly visible.

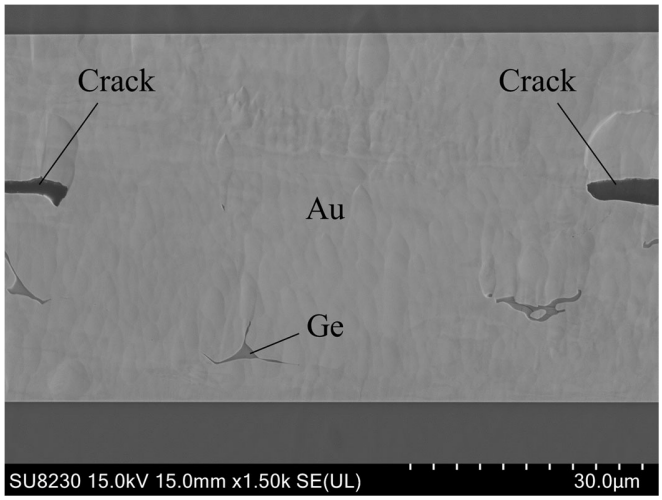

Fig. 8 SEM image of a cross section of a virgin sample from the high pressure, 7.6 MPa, group (b) after joining. A Au section extends across the through crack shown in Fig. 7 adjoining the substrate and the die with solid section.

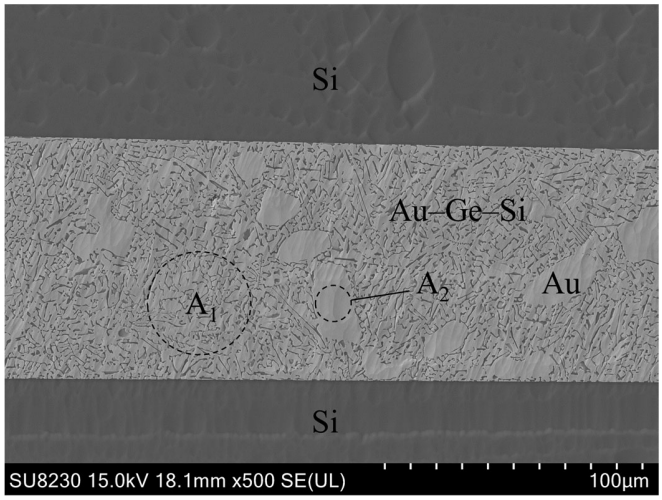

Fig. 9 SEM image of a cross section of a sample stored at 400 °C in N_2 for 1000 hours. The joint comprises a eutectic Au–Ge–Si compound with Au precipitates dispersed with in it. The light grey is Au and the dark grey is Ge–Si in the eutectic structure. The composition in regions A_1 and A_2 are given in Table II.

of small voids, or a through crack feature, were distinctly visible at the bond line (Fig. 7). Domains of Ge were found on both sides of the bond line. In some regions, relatively large sections of primary Au were extending across the bond line, as shown in Fig. 8.

The samples annealed at 400 °C for 1000 hours, group (c), showed a transformed microstructure, see Fig. 9. It had transformed into a morphology with a mainly eutectic type structure with two distinct phases or compounds; Au (primary α, light grey) and Ge–Si (solid solution, dark grey). There were

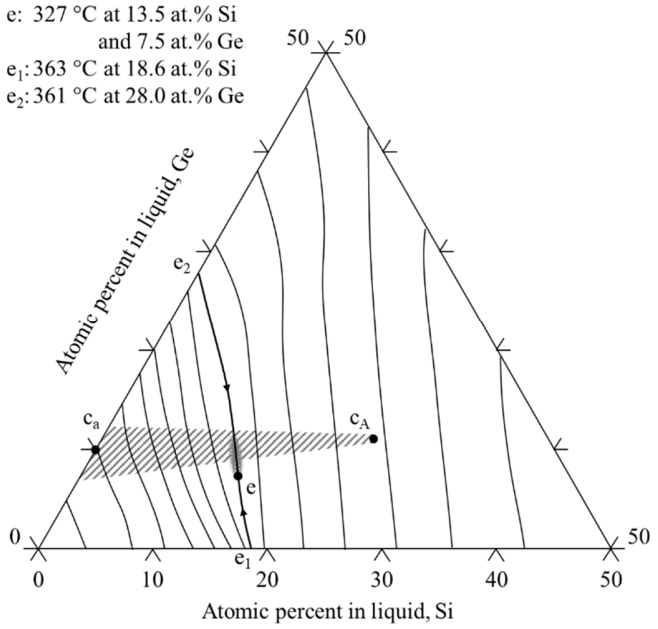

Fig. 10 The liquidus projection of the Au–Ge–Si ternary system. The Dashed region indicates a compositional transition path, from c_a to c_A, as Si diffuse into the joint. Note that the eutectic composition, e, and its melting point varies between sources between a composition comprising 11.7–14.0 at.% Si and 7.2–13.8 at.% Ge, and with a meting point between 326–357 °C [43]–[46]. This variation is indicated with a shaded area next to the eutectic point, e. The diagram was adapted from Harmelin, Elliott, and Okamoto, *et al.* [40], [46], [47].

also pure Au precipitates in the microstructure (domain A_2 in Table II). The eutectic type structure comprised roughly 65 at.% Au, 11 at.% Ge, and 24 at.% Si, see domain A_1 in Table II. This composition was a Si-rich off-eutectic composition of the ternary Au–Ge–Si system. The composition is indicated with a point, c_A, in the liquidus projection of the system depicted in Fig. 10.

Evidence for surface diffusion of Si from the periphery of the substrate was found on the substrate surface. Ge–Si dendrite structures with about 40 at.% Ge and 60 at.% Si was visible on the Au surface, as can be seen in Fig. 11. The laser cutting process had broken down the Ti layer around the periphery of the substrates and dies. This was visible in on the dies and substrates upon inspection. Substrates with a clear discoloration around their periphery are shown in Fig. 12. This is most likely due to the very high temperatures generated locally during the laser cutting process. Fig. 12 show the Si silicon distribution of a metalized and diced die after it had been exposed to one thermal cycle up to 380 °C, with a heating rate of 60 °C/min and cooling rate of 140 °C/min. There was a higher Si concentration around the periphery of the die than in the central part. This is assumed to have created a direct path for Si into the bond layer from the dies. On the fracture surface of one sample, a large area with Ge and Si was found, see Fig. 13. This indicates that the Ti layer might have catastrophically broken down during high-temperature storage. I.e., creating an additional diffusion path into the joint. Tungsten (W) has good diffusion barrier properties and was included in the adhesion/diffusion barrier layer during early development. Nonetheless, tungsten was omitted from the diffusion barrier

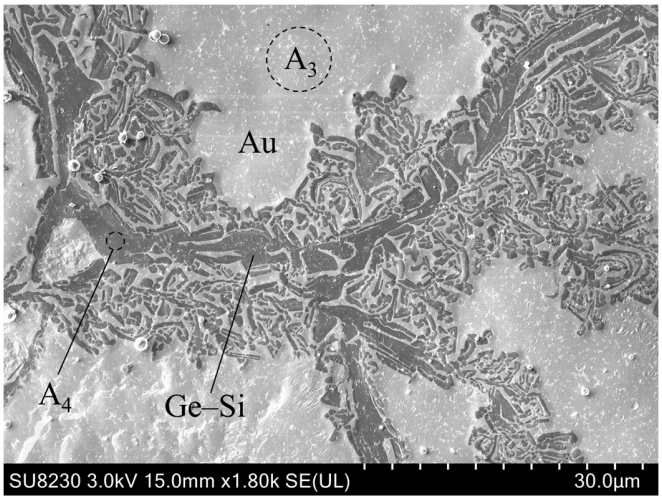

Fig. 11 Ge–Si dendrite type structure found on the substrate surface after exposure to a temperature above the melting point (400 °C). The composition in regions A_3 and A_4 are given in Table II.

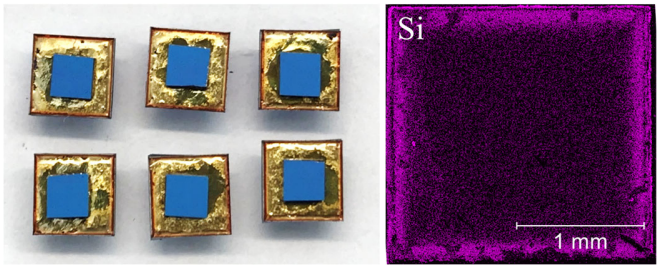

Fig. 12 Left: Virgin samples showing a dark, brown-red discoloration around the periphery of the substrate originating from the laser cutting process. The discoloration was found to be Si on the Au surface layer. Right: EDX map of the Si distribution on the surface of one die that has been exposed to one thermal cycle up to ~380 °C.

due to its poor influence on the adhesion characteristics on the layer. It is advised to commence a more detailed investigation on a suitable diffusion barrier. E.g., the possible inclusion of W into a TiW diffusion/adhesion barrier without compromising the adhesion too much.

B. Shear strength

All three shear tested groups showed a significant shear strength capacity, see Fig. 14. This is well beyond the requirement of at least 6 MPa as defined by MIL-STD-883H [27]. The shear strength results further showed that samples from group (a) were roughly 50% stronger than samples from group (b). The annealed group got stronger as Si diffused into the joint forming a new compound. All three groups showed a very similar fracture surface, see Fig. 15. An adhesive fracture was found between the Ti adhesion layer and the Si wafer on either the die or substrate side of the joint. In some samples, the fracture shifted from one adhesion layer, through the joint, to the other adhesion layer on the other side of the joint. Thus, the shear strength of the off-eutectic Au–Ge joint is at least in the magnitude order of 40–50 MPa as measured in this study. The measured strength is significantly lower than what is to be expected from regular eutectic Au–Ge joints, which typically show a shear strength of at least 50 MPa [7], [8], [28]–[30], and up to around 150 MPa have been reported [31]–[34]. Peal and scratch tests were performed

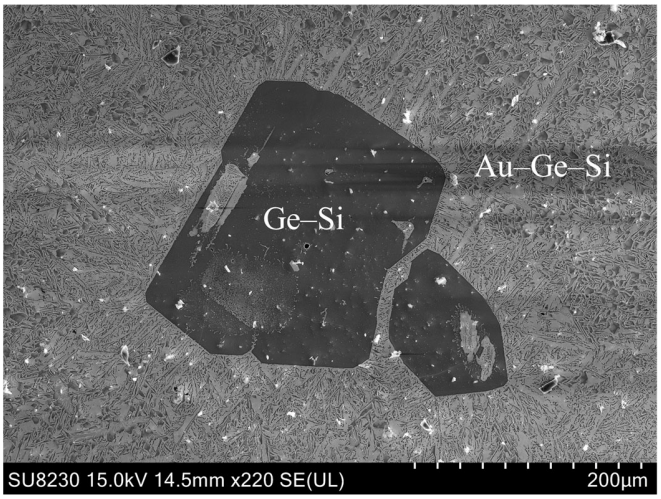

Fig. 13 Fracture surface of a sample annealed at 400 °C for 1000 hours, group (c). A large area where Ge and Si have diffused through the Ti adhesion/ diffusion barrier layer is shown. This causes an interdiffusion path for Si into the joint and for Ge into the die.

after deposition of the Ti and Au layers, before electroplating. The tests verified a very good adhesion of the metallization at that stage. Partial delamination of the metallization was discovered after dicing with a regular dicing saw. It was thought that the abrasive motion of the blade combined with the water jet caused the delamination. Thus, the dicing process was switched to a laser cutting process. Peel and scratch tests after dicing with laser cutting showed good adhesion. FEA results support this, as it shows a very high-stress state in the Ti layer at room temperature [25].

C. *Effective melting point*

Samples following the first heating regime (R_1) detached from the substrate at 460 ± 10°C. This is around 100 °C above the eutectic melting point of the binary Au–Ge material system, see Fig. 1. This is inside the two-phase field region where the joint is expected to be in a partially melted state. Samples following heating regime (R_2) showed completely different behavior. After around 10 min at 370–380 °C the die sheared off the substrate. This indicates that as Si diffuses into the joint a new Au–Ge–Si compound is formed. This new compound has a eutectic point about 34 °C lower than the eutectic melting point of Au–Ge, see Fig. 10. The liquid fraction of an incongruently melted off-eutectic Au–Ge compound comprising 8–12 at.% Ge at 370–380 °C would be roughly 19–37 %. This point is indicated with c_a in Fig. 1. Assuming that the compositional change evolves linearly from c_a (virgin) to the composition found in the annealed samples c_A, i.e., roughly 65 at.% Au, 11 at.% Ge, and 24 at.% Si, one sees that the composition passes very close to, or through, the eutectic melting point of the ternary system. This transition path is marked with a dashed region between c_a and c_A in Fig. 10. Thus, it is believed that as Si diffuses into the joint, a larger fraction of the joint liquifies until there is too little solid phase remaining to carry the mechanical load by the applied weight. That is why different heating regimes provide different results. For R_1, the high temperature accelerates the Si diffusion rapidly into the joint, while R_2 requires more time to get a similar composition.

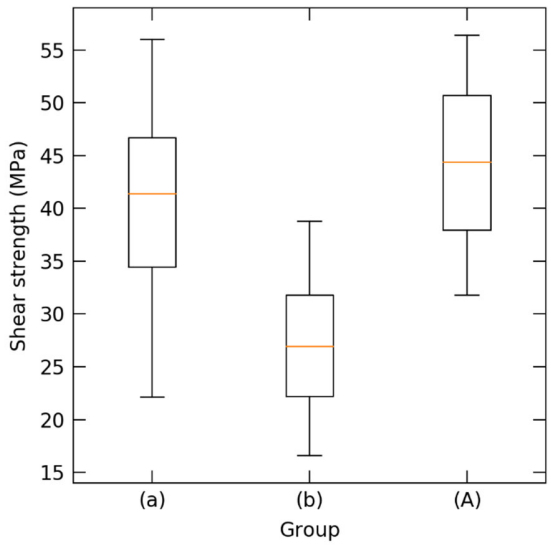

Fig. 14 Measured shear strength of three groups of samples: (a) Virgin samples bonded with a bond line pressure of 53 kPa, (b) Virgin samples bonded with a bond line pressure of 7.6 MPa, and (c) Samples bonded with a bond line pressure of 53 kPa and then stored at 400 °C in N_2 for 1000 hours.

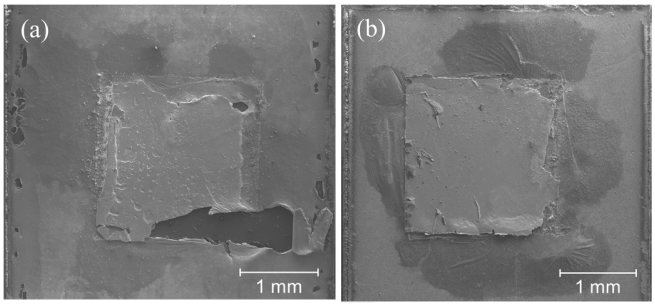

Fig. 15 SEM image of the fracture surface on the substrate of two samples after shear testing; (a) a sample from the low-pressure group (a), 53 kPa, and (b) a sample from the high-pressure group (b), 7.6 MPa. The dark areas around the joints are excess preform material squeezed out from the bond line during fabrication.

Elemental analysis and investigation of the fracture surfaces of samples from both test regimes support this explanation.

D. *Electrical Resistivity*

Fig. 16 shows the resistivity as a function of temperature for the strip of the eutectic preform. The graph shows a large step increase in resistivity at the point of melting. This coincided in time with visual observation of melting of the preform. Such a step is expected to be seen for the transition to a melted state, as liquid metal is known to have higher resistivity than solid [35], [36]. After the observed melting, the resistivity continues to increase with temperature, showing a time-dependent increase. This time dependence is believed to be due to an inhomogeneous distribution of Ge in the preform, resulting in gradual melting of the Au–Ge compound, caused by interdiffusion of Au and Ge. A similar step down in resistivity was observed as the sample was cooled, but it happens at a lower temperature, about 340 °C. This 21 °C offset in temperature between step up and down in resistivity may be explained by undercooling of the liquid phase before solidification [37], [38].

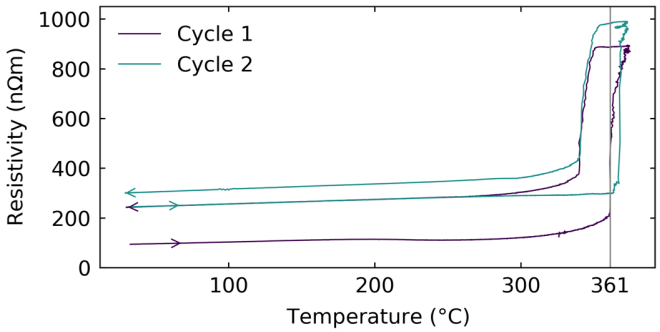

Fig. 16 Resistivity calculated from the resistance measurements of the preform sample over two thermal cycles. For the second cycle the sample had poor thermal contact with the substrate before melting.

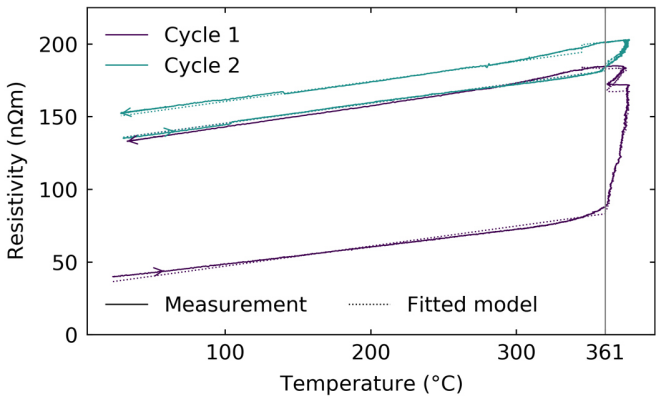

Fig. 17 Resistivity calculated from the resistance measurements of one sample over two thermal cycles. The artifact at high temperature in the first cycle was caused by a temperature drop due to a bug in the hot plate control. This occurred 6 min after reaching 361 °C for the first time.

For temperatures up to about 300 °C, the graph shows close to linear temperature dependence. However, there is an increase in resistivity after each thermal cycle, seen as a vertical shift in the graphs. For temperatures just below the step up or down in resistivity, the graph shows a higher resistivity than the linear dependence for lower temperature would predict. A possible explanation for this may be premelting; that a thin layer at the grain boundaries will be in a melted state even below the eutectic melting point [39].

In Fig. 17, resistivity is plotted as a function of temperature for one of the bonded samples. Compared to the graph for the preform, Fig. 16, this graph also shows a linear temperature dependence below 300 °C. For the first cycle, it starts with a resistivity and temperature coefficient slightly higher than those of pure Au. However, the bonded samples do not show the same type of distinct step increase and decrease in resistivity as was associated with the melting and solidification behavior of the preform. Inspection of the samples after thermal cycling showed clear evidence of a melting process. The bonded samples showed a strong time-dependent increase in resistivity as the temperature went past the eutectic melting point, 361 °C. This gives rise to the increase in resistivity seen after each thermal cycle, with a smaller increase after the second cycle. One sample was cycled five times, showing less increase in resistivity after each cycle. This time dependence might indicate an ongoing diffusion process which causes a microstructural change. Note that these samples had no Si wafer adjoined to the Au–Ge foil, hence there was no Si diffusion into the compound.

For the bonded samples, there was also an increase in resistivity just before reaching the eutectic melting point. However, this was only seen for the first thermal cycle. For the second thermal cycle, the resistivity in this region was less than what would be predicted by the linear dependence seen at lower temperatures. This may indicate an ongoing change in microstructure at this temperature. This microstructural change would likely lead to a final room temperature resistivity between the initial resistivity and the resistivity after one cycle.

The dependence of the resistivity on time in the partially melted state can be characterized by fitting a model to the measured data. Such a model could be based on adding a perturbation to a linear resistivity model for Au:

$$\rho(T, t_\mathrm{m}) = \rho_\mathrm{Au}(T) + \Delta\rho(T, t_\mathrm{m}) \qquad (1)$$

Where T is the temperature, and t_m is the total amount of time the sample has been in a partially melted state since the start of the experiment. The simple linear temperature dependence of Au is given by:

$$\rho_\mathrm{Au}(T) = \rho_0^\mathrm{Au}\left(1 + \alpha_\mathrm{Au}\left(T - T_0^\mathrm{Au}\right)\right) \qquad (2)$$

From [36], a value of 22.1 nΩm is found for ρ_0^Au at $T_0^\mathrm{Au} = 20$ °C, and a value of $3.91 \cdot 10^{-3}$ K^{-1} is calculated for α_Au for a temperature range up to 400 °C. The time dependence of the perturbation can be modeled as an exponential function, representing the solution of a first order differential equation with a time constant τ. As the graphs appear to be parallel in the linear region, the direct temperature dependence is modeled as proportional to the temperature. This gives

$$\Delta\rho(T, t_\mathrm{m}) = a(T - T_0) + \Delta\rho_0\left(1 - e^{-\frac{t_\mathrm{m}+t_0}{\tau}}\right), \qquad (3)$$

where a is the coefficient for the temperature dependence, with a reference temperature T_0, and $\Delta\rho_0$ is the resistivity perturbation at room temperature after infinite time. The time t_0 represents the state of the sample at the start of the measurement. It is related to, but not an exact measure of, the time spent in a partially melted state since bonding before the experiment. To account for a resistivity step at partial melting and solidification, separate values for $\Delta\rho_0$ are used depending on whether the sample is assumed to be in the partially melted or solid state, $\Delta\rho_0^\mathrm{s}$ and $\Delta\rho_0^\mathrm{m}$ respectively. In both cases, $T_0 = 25$ °C is used as the reference temperature.

Numerical optimization was used to fit the model parameters to the experimental data, using the sum of squared residuals as a cost function. Both Fig. 17 and Fig. 18 includes graphs for the fitted model parameters, showing that the model can be used to express the time dependence of the resistivity.

The fitted parameters vary between samples. Table III lists the range of some of the features of the graphs calculated from the fitted parameters. The average final resistivity of the samples was 0.17 μΩm. This value is considerably higher than for Au and can be explained by diffusion of Ge into the Au foil on both sides of the bond line. The fitted parameter for the step

TABLE III
RESULTS FROM MODEL FITTING

	Expression	Observed range	Unit
Final resistivity at T_0	$\rho_0^{\mathrm{Au}} + \Delta\rho_0^{\mathrm{s}}$	0.13 – 0.20	μΩm
Slope of linear region	$\Delta\rho_0^{\mathrm{m}} - \Delta\rho_0^{\mathrm{s}}$	0.13 – 0.17	nΩm/K
Step at partial melting	$a + \rho_0^{\mathrm{Au}}\alpha_{\mathrm{Au}}$	0.00 – 0.02	μΩm
Time constant	τ	5 – 17	min
Start time offset	t_0	1 – 4	min

in the resistivity indicates that a small step exists (partial melting), even if it is not clearly visible in the graph. The large range in the time constant may be in part due to uncertainty regarding the exact time of melting and solidification, as well as uneven temperature distribution in the samples. Still, it gives the order of magnitude of the rate of change of the resistivity with time spent in a partially melted state, i.e., most of the change happens during the first 5 to 10 minutes.

IV. CONCLUSIONS

Off-eutectic Au–Ge joints was investigated. A symmetrical Si / SiO_2 / Ti / Au / Au–Ge / Au / Ti / SiO_2 / Si configuration was used to investigate shear strength, microstructure, and evolution at 400 °C. Similar joints made with a Au / Au–Ge / Au configuration was used to characterize the electrical resistivity as a function of temperature above the eutectic melting point. Fracture analysis was carried out on the sheared surfaces. This study made the following findings:

- Fabricated joints with a bond line pressure of 53 kPa were of very high quality and comprised three types of microstructures
  - Layered Au / Au–Ge / Au with 10-20 at.% Ge
  - Layered Au / Au–Ge / Au with primary Au sections
  - Primary Au sections with 1-4 at.% Ge
- Joints fabricated with a bond line pressure of 7.6 MPa were flawed with a significant squeeze out during fabrication, creating Au–Au thermo-compression type joints with a through-crack and extensive voiding at the bond line.
- Samples annealed at 400 °C for 1000 hours showed that Si had diffused into the joint creating a eutectic type Au–Ge–Si structure with precipitates of Au.
- Shear tests revealed relatively strong joints, roughly ranging between 20–50 MPa, limited by the adhesion layer.
- The effecting melting point was measured to be up to at least 100 °C above the eutectic melting point (361 °C). Diffusion of Si into joint caused a compositional change until it reached a near eutectic composition of the ternary Au–Ge–Si with a melting point of 327 °C. At that stage, most of the material was melted, and no structural strength remained. Thus, the melting point of the fabricated off-eutectic Au–Ge joints could not be precisely quantified.
- Electrical resistivity measurements confirmed a melting process at the eutectic melting point by an abrupt increase in resistivity.
- The time dependent change in resistivity at elevated temperature is a strong indicator of a time dependent change in microstructure.

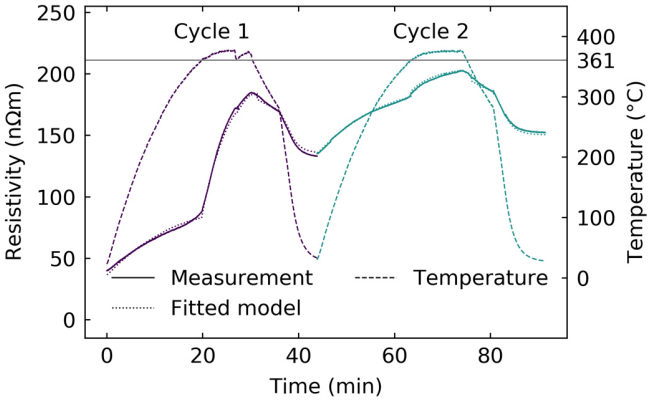

Fig. 18 Resistivity as function of time for one experiment, including the fitted model.

ACKNOWLEDGMENT

The authors would like to acknowledge Dr. Thai Anh Tuan Nguyen (sputtering), Zekija Ramic (electroplating), Thomas Martinsen, and Dr. Muhammad Tayyib for helping out in the lab at USN. The authors would also like to acknowledge Prof. Knut E. Aasmundtveit (USN), Dr. Torleif A. Tollefsen (TEGma AS) and Dr. Ole Martin Løvvik (SINTEF Industry) for their valuable support related to the project. Finally, they would like to send a special thanks to Thomas Aamli (TECHNI AS) for performing simulations for the project. And finally, we would to acknowledge Dr. Eric Beyne (IMEC) for his initial thoughts and ideas on electrical resistivity as a function of temperature.

REFERENCES

[1] M. S. Alam, J. C. Suhling, and P. Lall, "High Temperature Tensile and Creep Behavior of Lead Free Solders," in *16th IEEE Intersoc. Conf. on Therm. Thermomech. Phenom. Electron. Syst. (ITherm)*, Orlando, FL, USA, 2017, pp. 1229–1237.

[2] M. S. Alam, K. M. R. R. Hassan, J. C. Suhling, and P. Lall, "High temperature mechanical behavior of SAC and SAC+X lead free solders," in *IEEE 68th Electron. Compon. Technol. Conf. (ECTC)*, Las Vegas, NV, USA, 2018, pp. 1781–1789.

[3] H. S. Chin, K. Y. Cheong, and A. B. Ismail, "A Review on Die Attach Materials for SiC-Based High-Temperature Power Devices," *Metall. Mater. Trans. B*, vol. 41, no. 4, pp. 824–832, 2010.

[4] R. Kisiel and Z. Szczepański, "Die-attachment solutions for SiC power devices," *Microelectron. Reliab.*, vol. 49, pp. 627–629, 2009.

[5] V. R. Manikam and K. Y. Cheong, "Die attach materials for high temperature applications: a review," *Components, Packag. Manuf. Technol. IEEE Trans.*, vol. 1, no. 4, pp. 457–478, 2011.

[6] J. Cho, R. Sheikhi, S. Mallampati, L. Yin, and D. Shaddock, "Bismuth-Based Transient Liquid Phase (TLP) Bonding as High-Temperature Lead-Free Solder Alternatives," in *IEEE 67th Electron. Compon. Technol. Conf. (ECTC)*, Orlando, FL, USA, 2017, pp. 1553–1559.

[7] A. Drevin-Bazin, F. Lacroix, and J. F. Barbot, "SiC die attach for high-temperature applications," *J. Electron. Mater.*, vol. 43, no. 3, pp. 695–701, 2014.

[8] W. Sabbah, S. Azzopardi, C. Buttay, R. Meuret, and E. Woirgard, "Study of die attach technologies for high temperature power electronics: Silver sintering and gold-germanium alloy," *Microelectron. Reliab.*, vol. 53, no. 9–11, pp. 1617–1621, 2013.

[9] M. Patelka, N. Sakai, and C. Trumble, "Development of a Ag / glass die attach adhesive for high power and high use temperature applications," in *IMAPS Int. Conf. on High Temp. Election. (HiTEC)*, Albuquerque, NM, USA, 2016, pp. 123–127.

[10] L. A. Navarro *et al.*, "Thermomechanical assessment of die-attach materials for wide bandgap semiconductor devices and harsh environment applications," *IEEE Trans. Power Electron.*, vol. 29, no. 5, pp. 2261–

2271, 2014.
[11] S. Chen, C. Labarbera, and N. Lee, "Silver Sintering Paste Rendering Low Porosity Joint for High Power Die Attach Application," in *IMAPS Int. Conf. High Temp. Election. (HiTEC)*, Albuquerque, NM, USA, 2016, pp. 134–142.
[12] T. A. Tollefsen *et al.*, "Au-Sn SLID Bonding: A Reliable HT Interconnect and Die Attach Technology," *Metall. Mater. Trans. B*, vol. 44, no. 2, pp. 406–413, 2013.
[13] T. A. Tollefsen, O. M. Løvvik, K. Aasmundtveit, and A. Larsson, "Effect of temperature on the die shear strength of a Au-Sn SLID bond," *Metall. Mater. Trans. A*, vol. 44, no. 7, pp. 2914–2916, 2013.
[14] W. D. MacDonald and T. W. Eagar, "Transient Liquid Phase Bonding," *Annu. Rev. Mater. Sci.*, vol. 22, pp. 23–46, 1992.
[15] W. D. MacDonald and T. W. Eagar, "Transient liquid phase bonding processes," *Met. Sci. Join.*, pp. 93–100, 1992.
[16] W. D. MacDonald and T. W. Eagar, "Isothermal Solidification Kinetics of Diffusion Brazing," *Metall. Mater. Trans. A*, vol. 29A, no. January, pp. 315–325, 1998.
[17] W. F. Gale and D. A. Butts, "Transient liquid phase bonding," *Sci. Technol. Weld. Join.*, vol. 9, no. 4, pp. 283–300, 2004.
[18] G. O. Cook and C. D. Sorensen, "Overview of transient liquid phase and partial transient liquid phase bonding," *J. Mater. Sci.*, vol. 46, no. 16, pp. 5305–5323, 2011.
[19] L. Bernstein and H. Bartholomew, "Applications of Solid-Liquid Interdiffusion (SLID) Bonding in Integrated-Circuit Fabrication," *Trans. Metall. Soc. Aime*, vol. 236, no. 3, pp. 405–412, 1966.
[20] L. Bernstein, "Semiconductor Joining by the Solid-Liquid-Interdiffusion (SLID) Process," *J. Electrochem. Soc.*, vol. 113, no. 12, pp. 1282–1288, 1966.
[21] K. E. Aasmundtveit, T.-T. Luu, H.-V. Nguyen, A. Larsson, and T. A. Tollefsen, "Intermetallic bonding for High-Temperature Microelectronics and Microsystems: Solid-Liquid Interdiffusion Bonding," in *Intermetallic compounds - Formation and applications*, 1st ed., M. Aliofkhazrai, Ed. London: IntechOpen, 2018, pp. 43–72.
[22] K. S. Siow, "Are sintered silver joints ready for use as interconnect material in microelectronic packaging?," *J. Electron. Mater.*, vol. 43, no. 4, pp. 947–961, 2014.
[23] F. Yu, J. Cui, Z. Zhou, K. Fang, R. W. Johnson, and M. C. Hamilton, "Reliability of Ag Sintering for Power Semiconductor Die Attach in High-Temperature Applications," *IEEE Trans. Power Electron.*, vol. 32, no. 9, pp. 7083–7095, 2017.
[24] S. A. Paknejad and S. H. Mannan, "Review of silver nanoparticle based die attach materials for high power/temperature applications," *Microelectron. Reliab.*, vol. 70, pp. 1–11, 2017.
[25] A. Larsson, C. B. Thoresen, and T. Aamli, "Partially liquid interconnects with the Au–Ge system - Mechanical strength and electrical resistivity," in *Proc. Tech. Program - Pan Pac. Microelectron. Symp. (Pan Pacific)*, Kauai, HI, USA, 2019.
[26] B. Beekley, "Interface Evolution of Au-Au Thermocompression Bonding and Nanotwins," M.S. thesis, Univ. Calif., Los Angeles, CA, USA, 2015.
[27] "Test Method Standard - Microcircuits," 2010.
[28] S. Egelkraut, L. Frey, M. Knoerr, and A. Schletz, "Evolution of shear strength and microstructure of die bonding technologies for high temperature applications during thermal aging," in *IEEE 12th Proc. Electron. Packag. Technol. Conf. (EPTC)*, Singapore, 2010, pp. 660–667.
[29] F. Lang, S. Tanimoto, H. Ohashi, and H. Yamaguchi, "Long-term joint reliability of sic power devices at 330°C," in *Eur. Microelectron. Packag. Conf.*, Rimini, Italy, 2009, p. 5.
[30] F. Lang, H. Yamaguchi, H. Ohashi, and H. Sato, "Improvement in joint reliability of SiC power devices by a diffusion barrier between Au-Ge solder and Cu/Ni(P)-metalized ceramic substrates," *J. Electron. Mater.*, vol. 40, no. 7, pp. 1563–1571, 2011.
[31] S. Tanimoto, H. Tanisawa, K. Watanabe, K. Matsui, and S. Sato, "Power Module Package Structure Capable of Surviving Greater ΔTj Thermal Cycles," *Mater. Sci. Forum*, vol. 740–742, pp. 1040–1043, 2013.
[32] S. Tanimoto, K. Watanabe, H. Tanisawa, K. Matsui, and S. Sato, "Packaging techniques for compact SiC power modules operable in an extended Tj range," in *Electrochem. Soc. Meet., 224th*, San Francisco, CA, USA, 2013, p. 1.
[33] S. Tanimoto and K. Matsui, "High Junction Temperature and Low Parasitic Inductance Power Module Technology for Compact Power Conversion Systems," *IEEE Trans. Electron Devices*, vol. 62, no. 2, pp. 258–269, 2015.
[34] S. Tanimoto, K. Matsui, Y. Murakami, H. Yamaguchi, and H. Okumura, "Assessment of Au-Ge Die Attachment for an Extended Junction Temperature Range in Power Applications," in *IMAPS Int. Conf. High Temp. Election. (HiTEC)*, Albuquerque, NM, USA, 2010, pp. 32–39.
[35] C. Y. Ho *et al.*, "Electrical Resistivity of Ten Selected Binary Alloy Systems," *J. Phys. Chem. Ref. Data*, vol. 12, no. 2. pp. 183–322, 1983.
[36] R. A. Matula, "Electrical resistivity of Copper, Gold, Palladium, and Silver.pdf," *J. Phys. Chem. Ref. Data*, vol. 8, no. 4, pp. 1147–1298, 1979.
[37] A. Pasturel and N. Jakse, "Local order and dynamic properties in liquid Au-Ge eutectic alloys by ab initio molecular dynamics," *Phys. Rev. B*, vol. 84, no. 13, pp. 1–6, 2011.
[38] M. L. Kuntz, "Quantifying Isothermal Solidification Kinetics during Transient Liquid Phase Bonding using Differential Scanning Calorimetry," Ph.D. dissertation, Dept. Mech. Eng., Univ. Waterloo, Ontario, Canada, 2006.
[39] J. W. M. Frenken and J. F. Van Der Veen, "Observation of surface melting," *Phys. Rev. Lett.*, vol. 54, no. 2, pp. 134–137, 1985.
[40] H. Okamoto and T. B. Massalski, "The Au–Ge (Gold-Germanium) System," *Bull. Alloy Phase Diagrams*, vol. 5, no. 6, pp. 601–610, 1984.
[41] R. P. Elliott and F. A. Shunk, "The Au-Ge System (Gold-Germanium)," *Bull. Alloy Phase Diagrams*, vol. 1, no. 2, pp. 51–54, 1980.
[42] J. Wang, C. Leinenbach, and M. Roth, "Thermodynamic modeling of the Au-Ge-Sn ternary system," *J. Alloy. Compd.*, vol. 481, no. 1–2, pp. 830–836, 2009.
[43] Y. Jiang, "A computational thermodynamic model of Al-Au-Ge-Si quaternary system," B.S. thesis, Dept. Mater. Sci. Eng., Ohio State Univ., Columbus, OH, USA, 2011.
[44] S. Jin *et al.*, "Au-Ge Based Alloys for Novel High-T Lead Free Solder Materials – Fundamentals and Applications," in *Proc. Int. Brazing Soldering Conf., 5th*, Las Vegas, NV, USA, 2012, pp. 196–201.
[45] C. Leinenbach *et al.*, "Au-Ge-X (X = Cu , Ni) alloys for novel high-T lead-free solder materials," in *Discuss. Meet. thermodyn. Alloys*, Porto, Portugal, 2010.
[46] M. Harmelin, "Gold-Germanium-Silicon," in *Ternary alloys: Comp. Compend. Eval. Const. Data Phase Diagrams*, vol. 13, G. Effenberg, F. Aldinger, and A. Prince, Eds. VCH, 1995, pp. 45–54.
[47] R. P. Elliott and F. A. Shunk, "The Au-Si (Gold-Silicon) system," *Bull. Alloy Phase Diagrams*, vol. 4, no. 4, p. 362, 1983.

Andreas Larsson received his M.S. degree in engineering physics from Uppsala University in 2006. He became a Member (M) in 2011.

From 2006 to 2008 he worked as a calculation engineer within the Norwegian Oil & Gas industry. From 2008 to 2013 he has done research on packaging technology for harsh environments at SINTEF ICT in Oslo, Norway. Since 2013 he has been working with R&D on packaging technology, advanced multiphysics simulations and have held various management positions. He currently works as chief scientist at TECHNI AS in Borre, Norway, and are pursuing an industrial Ph.D. degree at the University of South-Eastern Norway. His current research interests include; packaging for harsh environments, thermoelectrics and thermomechanics.

Christian Bjørge Thoresen received the B.Sc. degree in electrical engineering from the University College of Southeast Norway (USN), Kongsberg, in 2008 and the M.Sc. degree in Microsystems technology from USN, Horten, in 2012. He is currently pursuing the Ph.D. degree at USN, Horten. His current interest of research is tangible user interface for capacitive touch screens.